MENTAL WORKLOAD CLASSIFICATION FROM SPATIAL REPRESENTATION OF FNIRS RECORDINGS USING CONVOLUTIONAL NEURAL NETWORKS

Marjan Saadati[1], Jill Nelson[2], Hasan Ayaz[3]

[1]Department of Electrical and Computer Engineering, George Mason University, Fairfax, VA
[2]Department of Electrical and Computer Engineering, George Mason University, Fairfax, VA
[3]School of Biomedical Engineering, Science and Health Systems, Drexel University, Philadelphia, PA
[1]msaadati@gmu.edu, [2]jnelson@gmu.edu, [3]hasan.ayaz@drexel.edu

ABSTRACT

Mental workload classification is a core element of designing adaptive Human-Computer Interfaces and plays an essential role in increasing the safety and operator performance of complex high-precision human-machine systems in fields such as aerospace and robotic surgery. Among non-invasive neuroimaging techniques, functional Near Infrared Spectroscopy (fNIRS) is a promising sensing modality for decoding mental states. While a variety of both classical and more modern classification techniques have been explored for fNIRS data, Convolutional Neural Networks (CNNs) have received only minimal attention. A significant advantage of CNNs compared to other classification methods is that they don't require prior feature selection or computationally demanding preprocessing. In previous studies on using CNN for fNIRS signals, temporal information from the fNIRS time series was emphasized, but valuable spatial information contained in the recordings was neglected. In this work, we propose and evaluate new structures for the image data fed to the CNN. We exploit the spatial information available in the fNIRS data by constructing images that retain spatial structure. Classification results on real datasets show a significant improvement (16% and 8%) compared to existing Support Vector Machine and Deep Neural Network methods.

Index Terms— Convolutional Neural Networks, Deep Learning, Mental Workload, Brain Computer Interfaces, fNIRS

1. INTRODUCTION

Human mental workload plays a critical role in many complex command and control systems. In recent decades, the advance of electronics has led to ever-growing complexity of machine functionality and interfaces ranging from military mission systems to civilian everyday tools. It is particularly important to track operator mental workload in situations where performance failures could result in catastrophic losses (e.g., surgery, air traffic control, etc.).

Accurate assessment of mental workload could help in preventing operator error and allow for pertinent intervention by predicting performance decline that can arise from either work overload or understimulation [1]. High cognitive demand of the interaction with a machine increases the likelihood of errors [2] by increasing reaction time, which is proportional to the number of parallel tasks and items to memorize [3]. Other consequences can be fatigue, cognitive capture, and oversight of critical information [3, 4]. Therefore, when aiming to enhance operator safety, mental workload assessment is necessary for adjusting the operator's workload to an optimal level [4]. The ability to continuously monitor the brains function carries an enormous potential to provide direct insight into user intentions and mental states [5].

Among the many invasive and noninvasive methods that have been used for measurement of neural activity, functional Near Infrared Spectroscopy (fNIRS) has demonstrated encouraging results toward higher accuracy in cognitive load classification and monitoring training [6, 7, 8]. fNIRS monitors the cortical hemodynamic responses that follow neuronal activity using wearable and portable hardware that includes near infrared light sources and detectors. Compared to electroencephalography (EEG), which monitors neurophysiological brain activity, fNIRS is less susceptible to electrical noise and movement artifacts but has lower temporal resolution and low depth resolution. However, the higher spatial resolution offered by fNIRS provides a better indication of which part of the cortex is activated.

Various fNIRS experiments for Brain-Computer Interface (BCI) and Human-Machine Interaction (HMI) applications have been investigated, including cognitive tasks [9, 10] and motor tasks [11, 12]. In many of these studies, feature extraction and machine learning algorithms are the primary focus, and SVM (Support Vector Machine) and LDA (Linear Discriminant Analysis) methods are frequently reported as the highest accuracy classifiers [13, 14]. One contrasting case is Aghajani et al. [3], who used SVM on a mental workload (MWL) experiment using hybrid fNIRS-EEG data and

978-1-7281-0824-7/19/$31.00 ©2019 IEEE

achieved 95% classification accuracy. However, performing MWL classification using conventional methods such as SVM requires a priori feature selection and preprocessing. The result depends on a variety of factors, including selecting the best set of features and size of the time window [12], and hence optimum classification is not guaranteed.

Deep Learning (DL) can overcome the challenge of feature selection, as it extracts features directly from the fNIRS signal and requires minimum feature preprocessing. However, DL for fNIRS-based classification has been applied in only a few studies, so much is still unknown. In 2016, Bashivan et al. [15] introduced a method to map the location of the electrodes to a 2D plane, building a topological image structure for representing EEG. They reported a best-performance accuracy of approximately 92%. In a study of motor imagery task classification (three classes) using hybrid EEG+fNIRS data, a 5-layer DNN was applied [16], and accuracy improvement of 10% compared to SVM and LDA methods was achieved. Most recently, the application of CNNs to fNIRs signals in the classification of a three-class motor execution task was investigated in [12]. An average of 6% improvement in classification was observed relative to SVM. Saadati et al. used DNN and CNN with a temporal framework for image construction for a variety of cognitive and motor tasks including n-Back, word generation and two-class motor imagery experiments. They reached to an average accuracy of 5% and 8% higher than SVM for DNN and CNN, respectively [17, 18].

To apply the CNN to time-series recordings, the time-series data must be converted to a 2D image for input to the CNN. In previous studies, a temporal approach is typically chosen for this step, i.e., capturing recordings of all fNIRS channels in a time window. The success of this method depends heavily on the length of the dataset and of the time window; a small number of samples could result in overfitting. In our work, we have investigated a different approach: spatial distribution of brain activity. In this approach, we build a 2D representation of the recorded time series based on the spatial coordinates of the channels. This method has two significant advantages over temporal representation: First, it retains and exploits the valuable spatial information in the fNIRS recordings. Second, the number of samples is large enough to achieve high classification accuracy and avoid overfitting even when the length of the experiment is short.

The remainder of the paper is organized as follows. Section 2 provides a brief description of CNNs. The proposed spatial representation of the fNIRS measurements is presented in Section 3. After a description of the dataset specifications and the dataset preprocessing in Section 4, the proposed CNN, including the network architecture and hyperparameter configuration, is described in Section 5. Finally, classification results are presented and discussed in Section 6, and Section 7 concludes the paper.

2. CONVOLUTIONAL NEURAL NETWORKS

The CNN is a multi-category classifier derived from Artificial Neural Networks (ANNs). A multi-category classification problem can be stated as the classification of N observation samples for each subject i, $\{\mathbf{X}_i, Y_i\}$. In this notation, $\mathbf{X}_i = [\mathbf{x}_{i1}, \ ... \ , \mathbf{x}_{ki} \ , ..., \ \mathbf{x}_{in}] \in \Re^{\mathbf{d}}$, where $\mathbf{x}_{ij}$ is the 2D image constructed from P channels at time j for subject i. $Y_i = [y_{i1} \ , y_{i2} \ , ..., \ y_{qi}, ..., \ y_{iC}] \in \Re^{\mathbf{C}}$ is the coded class. C is one of K distinct classes, e.g., for the n-back test with 3 levels, possible codes are 0, 1, and 2. The classifier function f, which maps the input images $\mathbf{x}_{ki}$ to the output label space is $f(\mathbf{X}_j; \theta) : \Re^{\mathbf{d}} \rightarrow C$ with estimation parameter θ.

In a CNN, the output of the function f is computed from a loss function based on the following conditional probability:

$$p(l_k | f_k(\mathbf{X}_j; \theta)) = \frac{exp(f_k(\mathbf{X}_j; \theta))}{\sum_{m=1}^{K}(exp(f_m(\mathbf{X}_j; \theta)))}. \qquad (1)$$

The loss function is given by

$$\theta^* = \underset{\theta}{\operatorname{argmin}} \sum_{j=1}^{N} \sum_{k=1}^{K} - \log(p(l_k | f_k(\mathbf{X}_j; \theta))) \delta(y_i = l_k), \qquad (2)$$

where $\delta(y_i = l_k)$ is the decision rule. Minimizing this loss function, the probability of each class determines the class of a sample [19].

2.1. The Architecture

A CNN applies convolution filters to the input data and solves a gradient descent problem with a smaller number of weights than an ANN. A CNN consists of several layers: the input layer, convolutional layer(s), max-pooling layer(s), fully connected hidden layer(s), and the output layer(s). The CNN used for the classification presented in this paper is shown in Fig. 1.a.

In the convolutional layer(s) of a CNN, a series of learnable convolution filters (kernels) are convolved across the raw pixel data of an image to extract and learn higher-level features. These higher-level features are called activation maps. The max-pooling layer downsamples the image data extracted by the convolutional layers to reduce the dimensionality of the feature map and decrease processing time.

The fully connected layer(s) perform classification on the extracted features based on information in labeled training data. Every node in a fully connected layer is connected to every node in the previous layer. Finally, the output layer contains a single node for each target class in the model with a softmax activation function to compute the probability of each class. The softmax activation function ensures that the final outputs fulfill the constraints of a probability density.

3. IMAGE STRUCTURE

To use a CNN for fNIRS-based MWL classification, the fNIRS signals from the brain must be converted to a data structure that can be fed into a deep learning algorithm. In the case of DNNs, this is an easy step since we are able to feed the time series directly into the first layer neurons of the network. In CNNs, however, the time-series signals need to be represented as 2D images, since this is the structure of the CNN input.

To convert the time-series data to images, snapshots of the recordings of all channels on the scalp are used to make a sample image. First, a mesh image is defined. At a given time (or sample) t_0, observations from the channels are inserted into the pixels corresponding to their spatial coordinates; values are assigned to the other pixels via linear interpolation. The example image below corresponds to the recording $\mathbf{S}^m_{t_0}$ at time t_0 with interpolated values $s^i_{t_0}$. The width and height of the image represent the spatial distribution of activity over the cortex. Performing this image construction procedure for each sample results in a grayscale topographical activity map which is used as the input image to the CNN. Unlike the temporal image method, this method preserves the spatial information while generating enough images to achieve strong classification performance.

$$\begin{bmatrix}
0 & 0 & s^i_{t_0} & s^i_{t_0} & s^i_{t_0} & s^i_{t_0} & s^i_{t_0} & s^i_{t_0} & s^i_{t_0} & 0 & 0 \\
0 & s^i_{t_0} & s^i_{t_0} & s^i_{t_0} & s^i_{t_0} & s^i_{t_0} & s^i_{t_0} & s^i_{t_0} & s^i_{t_0} & s^i_{t_0} & 0 \\
s^i_{t_0} & s^i_{t_0} & s^i_{t_0} & \mathbf{s}^1_{t_0} & s^i_{t_0} & \mathbf{s}^m_{t_0} & s^i_{t_0} & \mathbf{s}^m_{t_0} & s^i_{t_0} & s^i_{t_0} & s^i_{t_0} \\
s^i_{t_0} & s^i_{t_0} & \mathbf{s}^m_{t_0} & s^i_{t_0} & \mathbf{s}^m_{t_0} & s^i_{t_0} & \mathbf{s}^m_{t_0} & s^i_{t_0} & \mathbf{s}^m_{t_0} & s_{t_0} & s^i_{t_0} \\
s^i_{t_0} & s^i_{t_0} & s^i_{t_0} & \mathbf{s}^m_{t_0} & s^i_{t_0} & \mathbf{s}^m_{t_0} & s^i_{t_0} & \mathbf{s}^m_{t_0} & s^i_{t_0} & s^i_{t_0} & s^i_{t_0} \\
s^i_{t_0} & s^i_{t_0} & s^i_{t_0} & s^i_{t_0} & s^i_{t_0} & s^i_{t_0} & s^i_{t_0} & s^i_{t_0} & s^i_{t_0} & s^i_{t_0} & s^i_{t_0} \\
s^i_{t_0} & s^i_{t_0} & \mathbf{s}^m_{t_0} & s^i_{t_0} & s^i_{t_0} & s^i_{t_0} & s^i_{t_0} & \mathbf{s}^m_{t_0} & s^i_{t_0} & s^i_{t_0} & s^i_{t_0} \\
s^i_{t_0} & \mathbf{s}^m_{t_0} & s^i_{t_0} & \mathbf{s}^m_{t_0} & s^i_{t_0} & s^i_{t_0} & \mathbf{s}^m_{t_0} & s^i_{t_0} & \mathbf{s}^m_{t_0} & s^i_{t_0} & s^i_{t_0} \\
s^i_{t_0} & s^i_{t_0} & \mathbf{s}^m_{t_0} & s^i_{t_0} & s^i_{t_0} & \mathbf{s}^m_{t_0} & s^i_{t_0} & s^i_{t_0} & \mathbf{s}^m_{t_0} & s^i_{t_0} & s^i_{t_0} \\
0^i & s^i_{t_0} & s^i_{t_0} & s^i_{t_0} & \mathbf{s}^m_{t_0} & s^i_{t_0} & \mathbf{s}^m_{t_0} & s^i_{t_0} & s^i_{t_0} & s^i_{t_0} & 0 \\
0 & 0 & s^i_{t_0} & s^i_{t_0} & s^i_{t_0} & \mathbf{s}^m_{t_0} & s^i_{t_0} & s^i_{t_0} & s^i_{t_0} & 0 & 0
\end{bmatrix} \quad (3)$$

4. DATASET AND PREPROCESSING

4.1. Dataset

This study makes use of a dataset collected at the Technische Universitat Berlin by Jaeyoung Shin et al. [20] in 2017. The dataset includes simultaneous fNIRS (36 channels) recordings of the scalp for MWL during n-back (0-, 2- and 3-back) tasks. These tasks are classified into four possibilities: 0-, 2-, and 3-back tasks, and rest. The study included 26 right-handed healthy participants. The dataset consists of three sessions, where each session contains three series of 0-, 2-, and 3-back tasks. Nine series of n-back tasks were performed for each participant. A single series included 20 trials with 2 seconds for each trial (a total of 40 sec. task period), and a 20 sec. rest period in each session. Sixteen sources and 16 detectors were placed in frontal, motor, parietal, and occipital areas of the brain. A summary of the dataset is presented in Table 1.

Table 1. Summary of the data collected at the Technische Universitat Berlin by Jaeyoung Shin et al. [20] in 2017.

MWL	Trials	Task time	Rest time	Classification
n-Back	180	40	20	Level of difficulty

4.2. Preprocessing

The fNIRs data was sampled at a rate of 10 Hz. Deoxy- and Oxy-hemoglobin data, HbR and HbO, were computed from the fNIRS optical density using the modified Beer-Lambert law (mBLL) [20] using global baseline at the beginning of the session. The recording was filtered using a second-order digital Butterworth low pass filter with cut-off frequency of 0.08 Hz to remove the physiological noise due to motion artifacts, heart pulsation, and respiration. To calculate the HbR and HbO changes relative to rest, baseline correction was applied as the difference between the HbR and HbO, and the mean of the HbR and HbO in the rest period (base) prior to the window are calculated (Δ_{HbR} or Δ_{HbR}) and adapted to build images to feed to the CNN. For the spatial images, $\mathbf{S}^m_{t_0}$ is equal to the desired measure, i.e., either Δ_{HbR} or Δ_{HbR}.

5. PROPOSED CONVOLUTIONAL NEURAL NETWORK

A CNN with three convolutional layers (including max-pooling layers after each convolutional layer) and two fully connected layers is adapted to suit the given dataset. Its structure is shown in Fig. 1.a. The output layer consists of three units, with a softmax activation representing a probability distribution over the classes. This ensures that the network does not overfit by depending on specific hidden units. There are 32 3×3 kernels in each layer. The two fully connected layers have 256 and 128 neurons, respectively. This architecture was selected after experimenting with many different architectures, both shallower and deeper. Changes in image size as the data passes through the CNN are depicted in Fig. 1.a. The image size is 42×36; after three convolutional layers with a filter size of 3×3, the final image is 4×4. The activation function we use is the rectified linear unit (ReLU) function, considering its fast convergence and ability in dampening the vanishing gradient problem [19].

An overview of the entire classification process flow is shown in Fig. 1.b. After filtering, fNIRS data is squared, and then Δ_{HbO} is calculated. The data is fed to the CNN algorithm to train the network. This approach is not limited to mental workload classification and is general enough to be leveraged in any fNIRS-based classification task. The mental

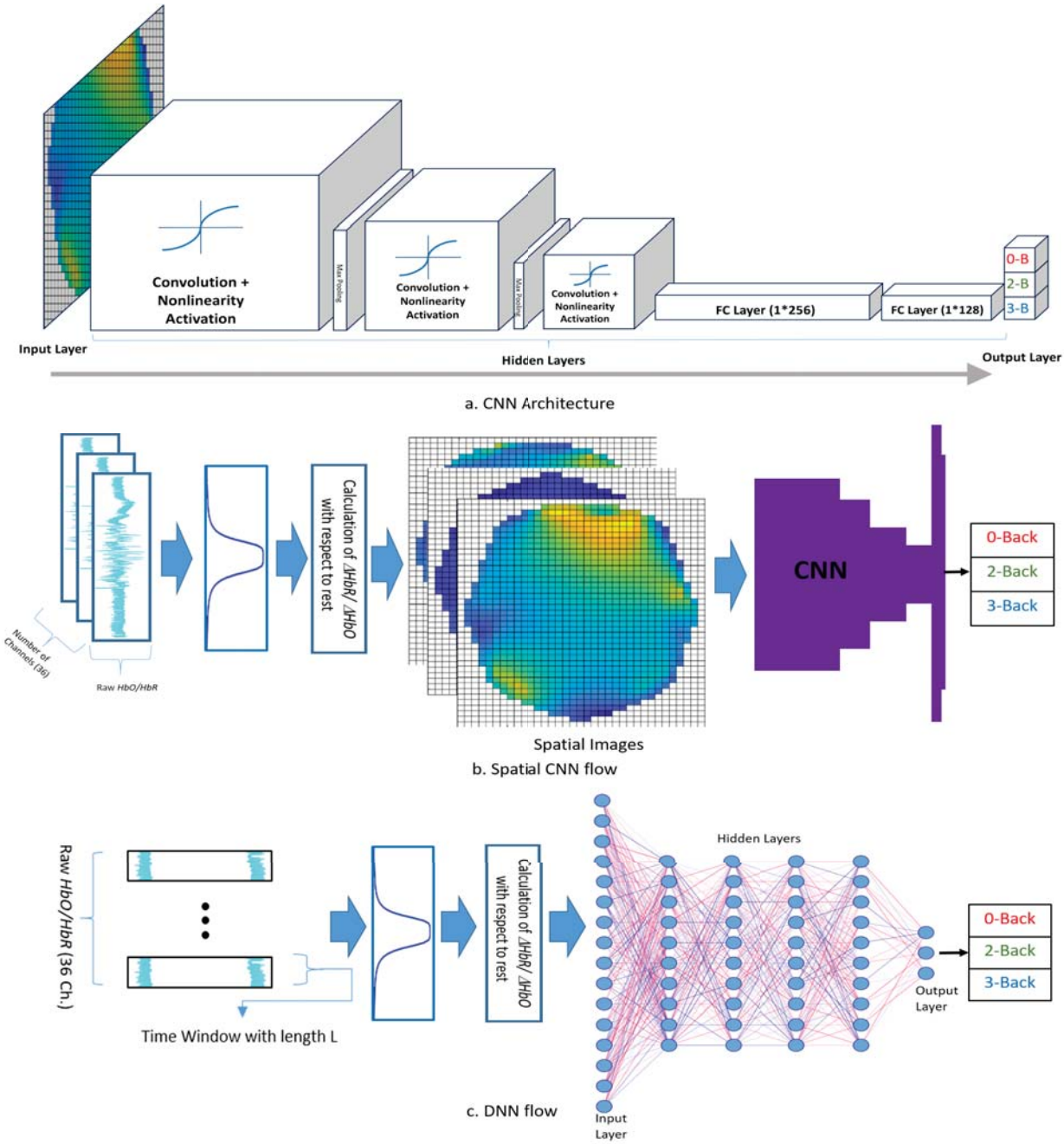

Fig. 1. a. Proposed network specifications: A CNN with three convolutional layers (including max-pooling after each convolutional layer), two fully connected layers, and a softmax output layer b. CNN classification process flow: After filtering, baseline correction and calculating Δ_{HbR} spatial representations are built and fed to the CNN algorithm to train the network. c. DNN classification process flow: Signals are divided into 1-sec. windows. After filtering, baseline correction and calculating Δ_{HbR} are fed to the DNN to train the network.

workload experiment serves as an example demonstrating the potential advantages of the approach.

6. CLASSIFICATION PERFORMANCE RESULTS

fNIRS data acquired from 26 human subjects has been denoised, and Δ_{HbR} and Δ_{HbO} have been calculated and la-

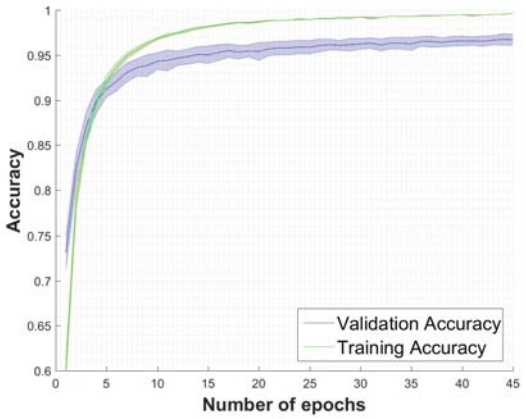

Fig. 2. Mean training and validation accuracy comparison over the number of the epochs

beled for 0-, 2-, and 3-back tasks. We compare performance across three classifiers: Spatial CNN, DNN, and SVM. Single subject classification mean accuracy and standard deviation for a 10-fold validation approach using Δ_{HbO} and each of the comparison classifiers are presented in Table 2. The DNN method, derived from [18], consists of four hidden layers, each with 60 neurons, shown in Fig. 1.c. The number of the neurons in the input layer is equal to the number of channels. The output layer consists of three classes with a soft-max activation. The input features to the DNN are defined as N samples, each of which contains values for Δ_{HbO} averaged over a 1-sec. time window for all channels [16]. The classification process flow for DNN is shown in Fig. 1.c; input features are calculated and filtered, then Δ_{HbO} is calculated and fed to the DNN algorithm to train the network.

For most subjects in the dataset, both of the deep learning classifiers (CNN and DNN) exhibit stronger classification performance than the SVM. Spatial CNN achieves considerably better classification performance than the other methods, reaching an average of 97% accuracy with a standard deviation of 1% for the Δ_{HbO} classification. This is a 16% improvement relative to SVM and an 8% improvement relative to DNN. A single subject best performance was achieved with the spatial CNN classifier with an accuracy of 99.6%.

A noted advantage of the spatial CNN is its low per-subject and between-subject standard deviation, 1%, which makes it a reliable classifier compared to the other methodologies which show 6% to 7% between-subject average standard deviation.

Figure 2 presents the accuracy for training and validation in Δ_{HbO}. The solid lines and shadowing illustrate the mean accuracy and standard deviation, respectively. As the figure indicates, the accuracy reaches its highest level around epoch 40 and then plateaus. Standard deviation of validation accuracy is higher than that of training during all of the training process, but it improves (declines) as the epoch number increases. Considering these measures, spatial CNN demonstrates a great potential for further use and investigation in fNIRS-based classification.

Table 2. Classification accuracy results for n-back tasks

Participants	1	2	3	4	5	6	7	8	9
Spatial CNN	0.98	0.89	0.97	0.95	0.99	0.97	0.99	0.99	0.97
SVM	0.82	0.8	0.76	0.76	0.87	0.71	0.8	0.84	0.8
DNN	0.91	0.7	0.82	0.86	0.83	0.81	0.96	0.92	0.85
Participants	10	11	12	13	14	15	16	17	18
Spatial CNN	0.99	0.91	0.98	0.94	0.97	0.92	0.99	0.96	0.97
SVM	0.91	0.78	0.91	0.67	0.82	0.87	0.93	0.78	0.84
DNN	0.89	0.89	0.89	0.77	0.93	0.83	0.95	0.83	0.85
Participants	19	20	21	22	23	24	25	26	**Avg.**
Spatial CNN	0.98	0.98	0.98	0.99	0.98	0.96	0.95	0.97	**0.97** $\pm$ **0.01**
SVM	0.84	0.91	0.8	0.87	0.78	0.93	0.84	0.89	**0.82** $\pm$ **0.06**
DNN	0.84	0.93	0.91	0.92	0.89	0.9	0.89	0.9	**0.87**$\pm$ **0.07**

7. CONCLUSION

We investigated the performance of a CNN structure with spatial data representation in the classification of mental workload using fNIRS data. The proposed algorithm significantly improves classification performance relative to a conventional SVM and a DNN, reaching 97% average accuracy for the n-back tasks, a 16% and 8% improved performance relative to the SVM and DNN, respectively. The results presented in this paper demonstrate the feasibility of achieving strong classification performance of fNIRS-based BCI using a CNN.

8. REFERENCES

[1] Raja Parasuraman and Matthew Rizzo, *Neuroergonomics: The Brain at Work*, Oxford University Press, 2008.

[2] John R Fedota and Raja Parasuraman, "Neuroergonomics and human error," *Theoretical Issues in Ergonomics Science*, vol. 11, no. 5, pp. 402–421, 2010.

[3] Haleh Aghajani, Marc Garbey, and Ahmet Omurtag, "Measuring mental workload with EEG+fNIRS," *Frontiers in Human Neuroscience*, vol. 11, pp. 359, 2017.

[4] Yichuan Liu, Hasan Ayaz, and Patricia A Shewokis, "Multisubject learning for mental workload classification using concurrent EEG, fNIRS, and physiological

measures," *Frontiers in human neuroscience*, vol. 11, pp. 389, 2017.

[5] Hasan Ayaz and Frédéric Dehais, *Neuroergonomics: The Brain at Work and in Everyday Life*, Academic Press, 2018.

[6] Alyssa M Batula, Youngmoo E Kim, and Hasan Ayaz, "Virtual and actual humanoid robot control with four-class motor-imagery-based optical brain-computer interface," *BioMed research international*, vol. 2017, 2017.

[7] Alyssa M Batula, Jesse Mark, Youngmoo E Kim, and Hasan Ayaz, "Developing an optical brain-computer interface for humanoid robot control," in *International Conference on Augmented Cognition*. Springer, 2016, pp. 3–13.

[8] Hasan Ayaz, Patricia A Shewokis, Scott Bunce, Kurtulus Izzetoglu, Ben Willems, and Banu Onaral, "Optical brain monitoring for operator training and mental workload assessment," *Neuroimage*, vol. 59, no. 1, pp. 36–47, 2012.

[9] Berdakh Abibullaev and Jinung An, "Classification of frontal cortex haemodynamic responses during cognitive tasks using wavelet transforms and machine learning algorithms," *Medical engineering & physics*, vol. 34, no. 10, pp. 1394–1410, 2012.

[10] Yichuan Liu, Elise A Piazza, Erez Simony, Patricia A Shewokis, Banu Onaral, Uri Hasson, and Hasan Ayaz, "Measuring speaker–listener neural coupling with functional near infrared spectroscopy," *Scientific Reports*, vol. 7, pp. 43293, 2017.

[11] Lei Wang, Adrian Curtin, and Hasan Ayaz, "Comparison of machine learning approaches for motor imagery based optical brain computer interface," in *International Conference on Applied Human Factors and Ergonomics*. Springer, 2018, pp. 124–134.

[12] Thanawin Trakoolwilaiwan, Bahareh Behboodi, Jaeseok Lee, Kyungsoo Kim, and Ji-Woong Choi, "Convolutional neural network for high-accuracy functional near-infrared spectroscopy in a braincomputer interface: three-class classification of rest, right-, and left-hand motor execution," *Neurophotonics*, vol. 5, pp. 5 – 5 – 15, 2007.

[13] Günther Bauernfeind, David Steyrl, Clemens Brunner, and Gernot R Müller-Putz, "Single trial classification of fNIRS-based Brain-Computer Interface mental arithmetic data: a comparison between different classifiers," in *2014 36th Annual International Conference of the IEEE Engineering in Medicine and Biology Society*. IEEE, 2014, pp. 2004–2007.

[14] Muhammad Raheel Bhutta and Keum-Shik Hong, "Classification of fNIRS signals for deception decoding using lda and svm," in *2013 13th International Conference on Control, Automation and Systems (ICCAS 2013)*. IEEE, 2013, pp. 1776–1780.

[15] Pouya Bashivan, Irina Rish, Mohammed Yeasin, and Noel Codella, "Learning representations from EEG with deep recurrent-convolutional neural networks," *arXiv preprint arXiv:1511.06448*, 2015.

[16] Antonio MM Chiarelli, Filippo Zappasodi, Francesco Di Pompeo, and Arcangelo Merla, "Simultaneous functional near-infrared spectroscopy and electroencephalography for monitoring of human brain activity and oxygenation: a review," *Neurophotonics*, vol. 4, no. 4, pp. 041411, 2017.

[17] Marjan Saadati, Jill Nelson, and Hasan Ayaz, "Multimodal fNIRS-EEG classification using deep learning algorithms for brain-computer interfaces purposes," in *Advances in Neuroergonomics and Cognitive Engineering*, Hasan Ayaz, Ed., Cham, 2020, pp. 209–220, Springer International Publishing.

[18] Marjan Saadati, Jill Nelson, and Hasan Ayaz, "Convolutional neural network for hybrid fNIRS-EEG mental workload classification," in *Advances in Neuroergonomics and Cognitive Engineering*, Hasan Ayaz, Ed., Cham, 2020, pp. 221–232, Springer International Publishing.

[19] Robin Tibor Schirrmeister, Jost Tobias Springenberg, Lukas Dominique Josef Fiederer, Martin Glasstetter, Katharina Eggensperger, Michael Tangermann, Frank Hutter, Wolfram Burgard, and Tonio Ball, "Deep learning with convolutional neural networks for EEG decoding and visualization," *Human brain mapping*, vol. 38, no. 11, pp. 5391–5420, 2017.

[20] Jaeyoung Shin, Alexander Von Lhmann, Do-Won Kim, Jan Mehnert, Han-Jeong Hwang, and Klaus-Robert Müller, "Simultaneous acquisition of EEG and nirs during cognitive tasks for an open access dataset," *Scientific data*, vol. 5, pp. 180003, 2018.

[21] M. Saadati and J. K. Nelson, "Multiple transmitter localization using clustering by likelihood of transmitter proximity," in *2017 51st Asilomar Conference on Signals, Systems, and Computers*, Oct 2017, pp. 1769–1773.

[22] A. Pourshafie, S. S. Mortazavi, M. Saniei, M. saadati, and A. Saidian, "Optimal reactive power compensation in a deregulated distribution network," in *2009 44th International Universities Power Engineering Conference (UPEC)*, Sep. 2009, pp. 1–6.